Long-lived keratin 15+ esophageal progenitor cells contribute to homeostasis and regeneration

Véronique Giroux,[1,2] Ashley A. Lento,[1,2] Mirazul Islam,[3] Jason R. Pitarresi,[1,2] Akriti Kharbanda,[1,2] Kathryn E. Hamilton,[1,2] Kelly A. Whelan,[1,2] Apple Long,[1,2] Ben Rhoades,[1,2] Qiaosi Tang,[1,2] Hiroshi Nakagawa,[1,2] Christopher J. Lengner,[4] Adam J. Bass,[3,5] E. Paul Wileyto,[6] Andres J. Klein-Szanto,[7] Timothy C. Wang,[8] and Anil K. Rustgi[1,2,9]

[1]Division of Gastroenterology, Department of Medicine, and [2]Abramson Cancer Center, University of Pennsylvania, Philadelphia, Pennsylvania, USA. [3]Department of Medical Oncology, Dana-Farber Cancer Institute, Boston, Massachusetts, USA. [4]Department of Biomedical Sciences, School of Veterinary Medicine, and Institute for Regenerative Medicine, University of Pennsylvania, Philadelphia, Pennsylvania, USA. [5]Harvard Medical School, Boston, Massachusetts, USA. [6]Department of Biostatistics and Epidemiology, University of Pennsylvania, Philadelphia, Pennsylvania, USA. [7]Department of Pathology and Cancer Biology Program, Fox Chase Cancer Center, Philadelphia, Pennsylvania, USA. [8]Division of Digestive and Liver Disease, Department of Medicine, Columbia University, New York, New York, USA. [9]Department of Genetics, University of Pennsylvania, Philadelphia, Pennsylvania, USA.

The esophageal lumen is lined by a stratified squamous epithelium comprised of proliferative basal cells that differentiate while migrating toward the luminal surface and eventually desquamate. Rapid epithelial renewal occurs, but the specific cell of origin that supports this high proliferative demand remains unknown. Herein, we have described a long-lived progenitor cell population in the mouse esophageal epithelium that is characterized by expression of keratin 15 (*Krt15*). Genetic in vivo lineage tracing revealed that the *Krt15* promoter marks a long-lived basal cell population able to self-renew, proliferate, and generate differentiated cells, consistent with a progenitor/stem cell population. Transcriptional profiling demonstrated that *Krt15*$^+$ basal cells are molecularly distinct from *Krt15*$^-$ basal cells. Depletion of *Krt15*-derived cells resulted in decreased proliferation, thereby leading to atrophy of the esophageal epithelium. Further, *Krt15*$^+$ cells were radioresistant and contributed to esophageal epithelial regeneration following radiation-induced injury. These results establish the presence of a long-lived and indispensable *Krt15*$^+$ progenitor cell population that provides additional perspective on esophageal epithelial biology and the widely prevalent diseases that afflict this epithelium.

Introduction

Adult tissues undergo cellular renewal at variable rates. In some tissues, such as blood, skin, and intestine, stem cells are the source of new cells. In other tissues, such as the kidney, stem cells do not appear to play an appreciable role during homeostasis. In some contexts, a small population of differentiated cells called facultative stem cells can acquire a "stem cell–like" identity to regenerate and repair tissue following injury (1).

Stem cells are defined as self-renewing, multipotent cells that can give rise to all differentiated lineages within a tissue. Thus, they are the principal cell type within the cellular hierarchy for normal homeostasis and tissue regeneration following injury, such as infection, inflammation, chemotherapy, and radiation. Interestingly, in tissues with high cell turnover, as illustrated in the hair follicle, the hematopoietic system, and the small intestine, 2 major classes of molecularly and functionally distinct stem cells are present. The first class is a fast-cycling population that rapidly produces progeny to support the general maintenance of tissue function. The second class is a slower-cycling "reserve" population that replenishes the faster-cycling stem cell pool during homeostasis and following injury (2–4). Stem cells are generally supported by a unique environmental niche that regulates their activity and behavior. For example, Paneth cells and the surrounding mesenchyme are important constituents of the small intestinal stem cell niche (5, 6); the dermal papilla and dermal fibroblasts are critical in the hair follicle niche (7); and the perisinusoidal bone marrow niche is important for hematopoietic stem cells (8).

The esophageal lumen is lined by a stratified squamous epithelium characterized by proliferative cells restricted to the basal layer. Basal cells migrate toward the luminal surface while undergoing early differentiation (suprabasal cells) and terminal differentiation (superficial squamous cells). These cells eventually desquamate into the lumen. The esophageal epithelium undergoes relatively rapid renewal. Each of the epithelial cellular compartments is distinguished by different morphological features (round versus elongated cells, variable nuclear/cytoplasmic ratio, and keratin content) and divergent expression of key proteins. Esophageal basal cells are annotated by SOX2 and p63 expression, as well as expression of keratins 5 and 14, the latter forming intermediate filaments. Suprabasal cells are characterized by the expression of keratins 4 and 13, as well as involucrin. Superficial squamous cells harbor keratohyaline granules with profilaggrin and filaggrin. In aggregate, the proliferative basal cells, and early-differentiating suprabasal cells, and terminally differentiated superficial squamous cells represent distinct states of lineage commitment.

It is likely that long-lived cells with properties consistent with stem/progenitor cells reside in the basal compartment of the

Conflict of interest: The authors have declared that no conflict of interest exists.
Submitted: June 8, 2016; **Accepted:** March 9, 2017.
Reference information: *J Clin Invest.* 2017;127(6):2378–2391.
https://doi.org/10.1172/JCI88941.

esophageal epithelium. Although their existence has been suggested through label-retaining studies and 3D organoid culture assays, their true identity remains to be fully described (9–14). We reported previously that a side population of mouse esophageal basal cells is capable of DNA label retention and also excludes Hoechst dye, a feature associated with the presence of ATP-binding cassette membrane transporters that has been linked to stem cell activity in several tissues (e.g., hematopoietic stem cells) (15). Furthermore, these cells give rise to undifferentiated and differentiated cells in 3D organotypic culture (12). Potential cellular heterogeneity in mouse esophageal basal cells was also reported by another group using an additional 3D culture system (11). These basal cells harbor different cell cycle and proliferation kinetics, leading to the suggestion that a nonquiescent putative stem cell population ($ITGA6^{hi}ITGB4^{hi}CD73^{+}$) resides in the basal layer. These 2 studies support the possibility of a stem cell population(s) in the mouse esophagus. Conversely, 1 study found no evidence of slow-cycling epithelial stem cells in the mouse esophagus, and suggested that each cell within the basal cell layer is equipotent in generating both proliferating and differentiating cells with equal probability (10). This equipotent model has also been reported for the stratified epithelium of the skin (16).

Genetic lineage tracing remains the gold standard approach for demonstrating self-renewal and multipotency and thus validating the identity of tissue-specific stem cells (17). In the esophagus, these approaches are required to establish the existence and identity of stem cells and to characterize their self-renewal and multipotency properties. This is critical for our understanding of the cellular basis of widely prevalent esophageal diseases, such as acid reflux–induced esophagitis, eosinophilic esophagitis, and esophageal carcinoma (18, 19).

Morphological similarities between the epidermis and the esophageal epithelium suggest that comparable stem cell populations could be present in both tissues. Lineage tracing experiments in the mouse skin have demonstrated that the *Krt15* (keratin 15) promoter marks cells in the bulge of the hair follicle that can generate all epithelial lineages (20). Interestingly, $Krt15^{+}$ cells in the hair follicle contribute to wound repair and squamous papilloma development in mice (21, 22). Basal cell carcinomas also arise from the hair follicle and more specifically from the $Krt15^{+}$ cells (23). Furthermore, *Krt15* also marks the ureter epithelium, and its expression is increased in a subset of urothelium cell carcinomas (24). Given its critical role in epidermal renewal, repair, and cancer development, investigation of $Krt15^{+}$ cells may provide critical insights into a putative esophageal stem cell population. Notably, the keratin 15 protein (K15) is a type I acidic cytokeratin expressed in the esophageal basal cell layer that pairs with keratin 5 in the postnatal period of young mice.

In the current study, we demonstrate that the activity of the *Krt15* promoter (using *Krt15-CrePR1* $R26^{mT/mG}$ and *Krt15-CrePR1* $R26^{Confetti}$ mice) (20, 25, 26) identifies a long-lived subpopulation of basal cells in the mouse esophagus capable of generating all states of squamous lineage commitments. Self-renewal of $Krt15^{+}$ cells is corroborated through a 3D organoid culture system and long-term in vivo lineage tracing. RNA sequencing (RNA-Seq) reveals a distinct transcriptional profile of $Krt15^{+}$ basal cells relative to $Krt15^{-}$ basal cells, and Gene Set Enrichment Analysis (GSEA) demonstrates enrichment for gene sets associated with stem cell proliferation and cell fate in the $Krt15^{+}$ basal cell population. Genetic ablation of $Krt15^{+}$ cells using an inducible diphtheria toxin receptor allele ($R26^{iDTR}$) results in reduced proliferation and epithelial atrophy. Furthermore, $Krt15^{+}$ cells are radioresistant and contribute to tissue regeneration. Collectively, our studies establish the identity of a bona fide esophageal epithelial long-lived progenitor cell population that will underpin future approaches for the investigation and treatment of benign and malignant esophageal diseases.

Results

Krt15 marks a long-lived basal cell subpopulation in the mouse esophagus. *Krt15* mRNA and K15 protein are expressed in the adult mouse esophagus and in other stratified epithelia of the upper digestive tract, such as the forestomach and tongue (Supplemental Figure 1, A and B; supplemental material available online with this article; https://doi.org/10.1172/JCI88941DS1). Immunohistochemical staining reveals that endogenous K15 expression is restricted to the basal compartment of these tissues. Indeed, K15 is detected in basal cells labeled with the transcription factor p63 and in proliferative cells labeled with Ki-67, but is not detected in suprabasal cells labeled with keratin 13 (K13) (Figure 1A). K15 is expressed also in the embryonic esophagus (Supplemental Figure 1C) and the newborn mouse esophagus, forestomach, and tongue (Supplemental Figure 1D). Despite the morphological and functional differences between the mouse and the human esophagus, we detect K15 in a subset of the basal cells of normal esophageal biopsies. 3D organoids derived from normal human esophagus also express K15 (Supplemental Figure 1E).

The *Krt15* promoter marks long-lived cells in the hair follicle (20, 27) as well as in sweat glands (28), suggesting that $Krt15^{+}$ cells may have stem cell potential in other epithelia. We thus used a genetic lineage tracing approach to study the esophageal epithelial cells in which the *Krt15* promoter is active. The progesterone receptor–fused (PR1-fused) Cre allele *Krt15-CrePR1* (20) was bred into mice containing a $ROSA26^{mTomato/mEGFP}$ ($R26^{mT/mG}$) (25) allele, in which Cre recombination, induced by the PR agonist RU486, induces a switch from tdTomato to GFP expression. *Krt15-CrePR1* $R26^{mT/mG}$ mice were given a single dose of RU486, and the esophagi, forestomachs, and tongues were harvested 1 day later (D1) (Figure 1B). GFP^{+} ($Krt15^{+}$) cells were counted and localized (basal, parabasal [i.e., contiguous to a particular basal cell], suprabasal, or superficial cells) (Supplemental Figure 2A). Labeling occurred almost exclusively in basal and parabasal cells (Figure 1, B and C). The percentage of GFP^{+} cells in the basal layer (recombination rate) of the esophageal epithelium was 0.4%, suggesting that the *Krt15* promoter marks a subpopulation of cells in the basal layer (Supplemental Figure 2B). Next, 5 consecutive daily RU486 injections were administered to perform lineage tracing experiments (Figure 1D). Under these conditions, the percentage of GFP^{+} cells in the basal layer increased to 13.6% at D1 (1 day after the last RU486 injection) because of a higher recombination rate and also division of the originally recombined cells (Supplemental Figure 2B). In the lineage tracing experiment, GFP-labeled cells were detected at multiple time points (from D1 to D56 following recombination) in the esophagus (Figure 1E) as well as in the forestomach (Supplemental Figure 2C) and the

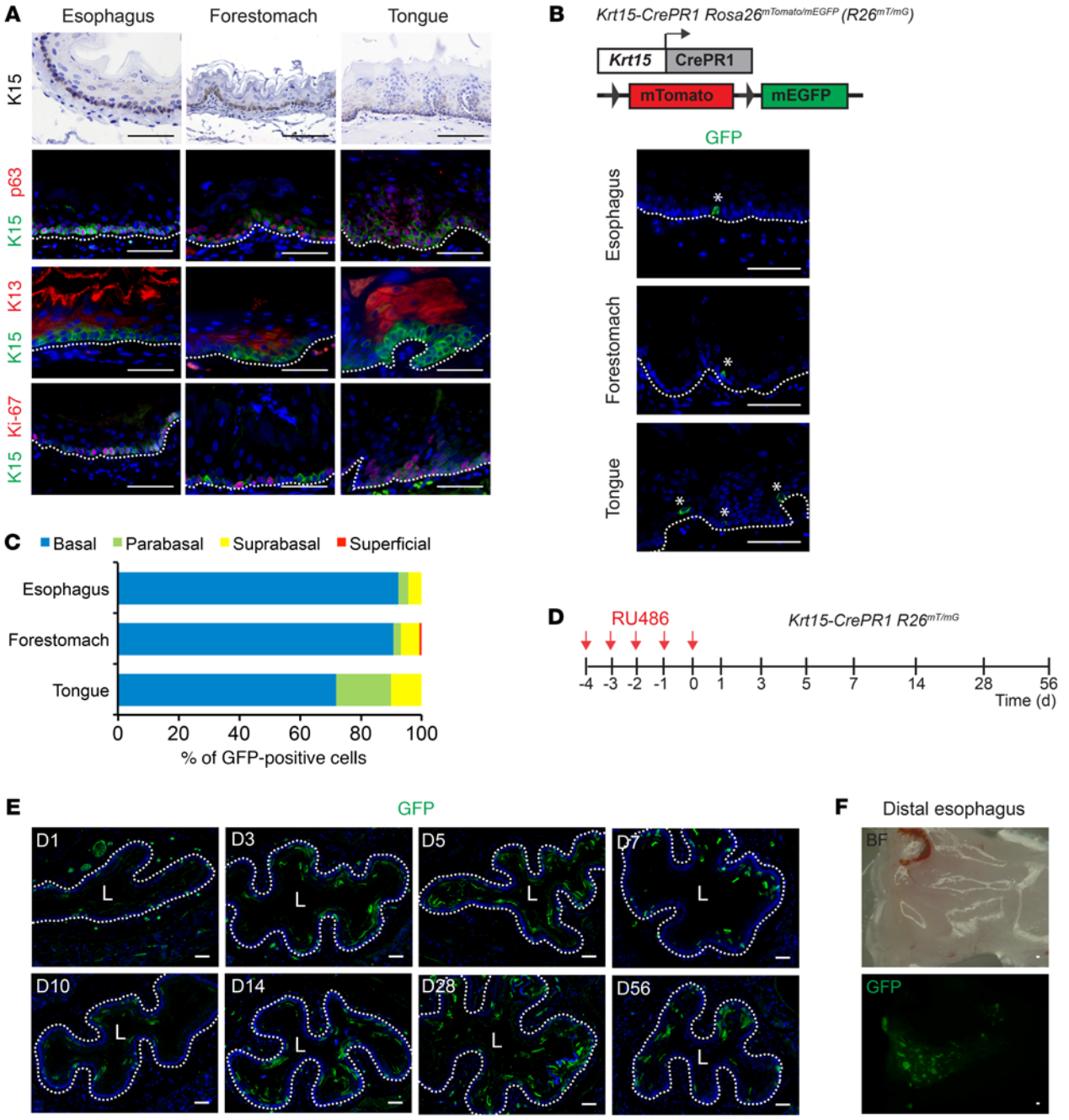

Figure 1. *Krt15* marks long-lived basal cells in the mouse esophageal epithelium. (**A**) Top panels: Localization of K15 in the mouse esophagus, forestomach, and tongue. Lower panels: Colocalization of K15 with p63, K13, or Ki-67 used as basal, suprabasal, and proliferative cell markers, respectively. (**B** and **C**) *Krt15-CrePR1 R26*$^{mT/mG}$ mice were injected with 0.5 mg RU486 and sacrificed 24 hours later. (**B**) Localization of GFP-labeled (*Krt15*$^{+}$) cells in mouse esophageal, forestomach, and tongue epithelia. Asterisks indicate recombined cells. (**C**) Graph represents the percentage of total GFP cells localized in each compartment (mean of 4 mice; cross sections of 4 different regions of the esophagus were analyzed for each mouse). (**D**–**F**) *Krt15-CrePR1 R26*$^{mT/mG}$ mice were injected daily with 0.5 mg RU486 for 5 consecutive days and sacrificed at listed time points. (**D**) Schematic illustration of RU486 treatments and sacrifice times for the genetic lineage tracing experiments. (**E**) GFP (*Krt15*$^{+}$ cells) immunofluorescence in esophageal sections of *Krt15-CrePR1 R26*$^{mT/mG}$ mice. (**F**) Whole-mount esophagus imaging of *Krt15-CrePR1 R26*$^{mT/mG}$ mouse sacrificed 6 months after Cre recombination. "L" indicates the lumen; dotted line marks the basement membrane. Scale bars: 50 μm.

tongue (Supplemental Figure 2D). Expansion of the GFP-labeled cells in the shorter induction was followed by maintenance of the GFP-labeled population in the later induction (Figure 1E and Supplemental Figure 2, C and D). Whole-mount esophagus imaging of *Krt15-CrePR1 R26*$^{mT/mG}$ mice 180 days following recombination demonstrates that the *Krt15* promoter marks long-lived cells in the esophagus (Figure 1F). Costaining of GFP^{+} cells with a K15-specific antibody in *Krt15-CrePR1 R26*$^{mT/mG}$ mice sacrificed at D1 confirmed the specificity of the *Krt15* promoter activity (Supplemental Figure 3A). These lineage tracing experiments demon-

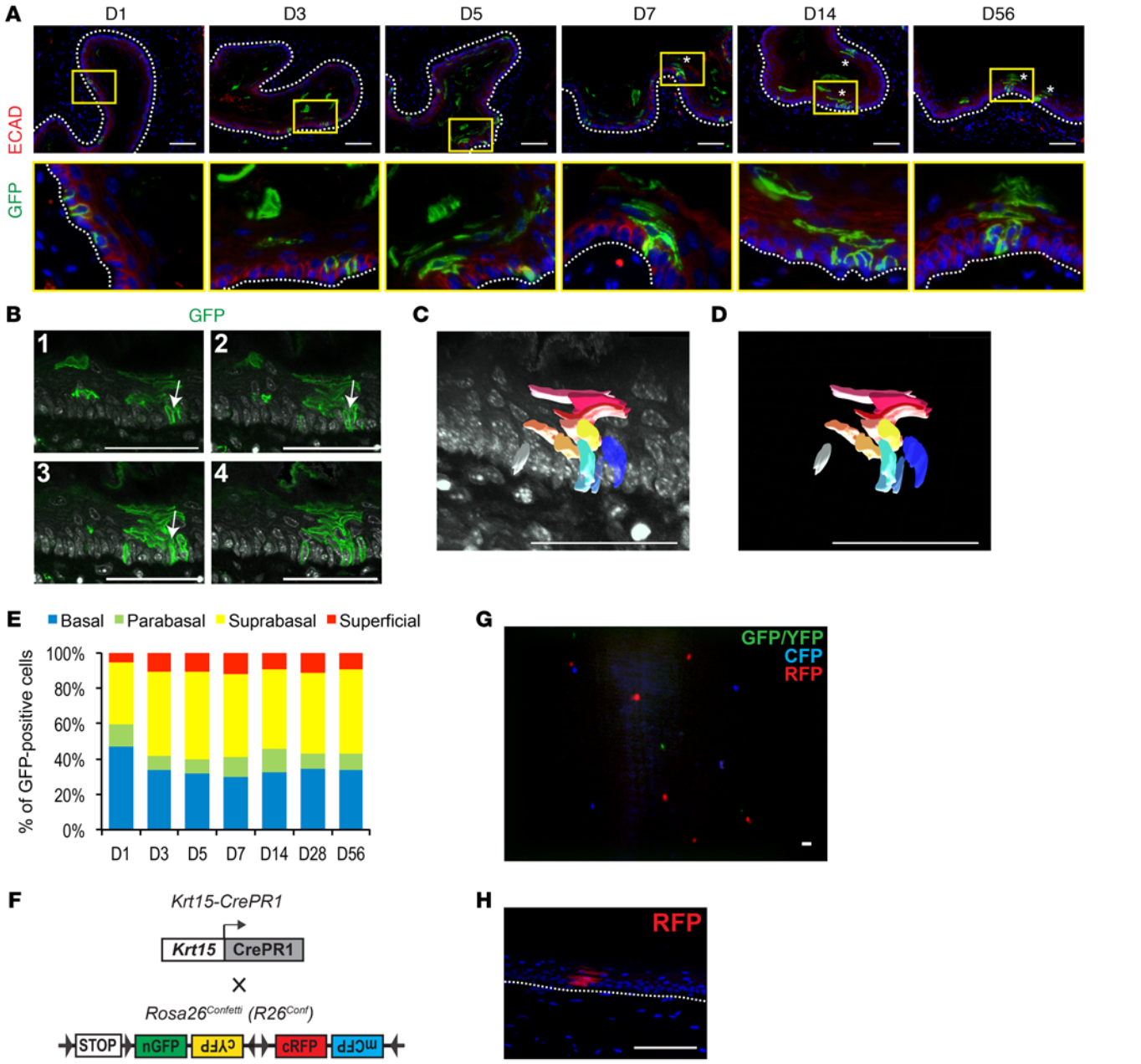

Figure 2. Basal *Krt15*⁺ cells undergo division initially and migrate toward the lumen. (**A**) *Krt15-CrePR1 R26*$^{mT/mG}$ mice were injected daily with 0.5 mg RU486 for 5 consecutive days and sacrificed at listed time points. Esophageal sections were stained for GFP (*Krt15*⁺ cells) and E-cadherin (ECAD). Clonal units are marked by an asterisk. Bottom panels represent magnification of regions of interest identified by a yellow rectangle in the top panels. (**B**–**E**) *Krt15-CrePR1 R26*$^{mT/mG}$ mice were injected daily with 0.5 mg RU486 for 5 consecutive days and sacrificed 56 days after the last day of recombination. One-hundred-micrometer sections were stained with GFP (*Krt15*⁺ cells) and imaged by confocal microscopy. (**B**) Single-plane images 3.3 μm apart from a Z-stack. Arrows mark a GFP⁺ cell emerging from the basal layer. (**C** and **D**) 3D reconstruction of a clonal unit marking basal cells in blue, suprabasal cells in red, and a parabasal cell in yellow. A single basal cell not part of the clonal unit is labeled in white. Gray, DAPI. (**E**) Graph represents the percentage of total GFP⁺ cells localized in each layer (mean of 4 mice; cross sections of 4 different regions of the esophagus were analyzed for each mouse; minimum of 400 GFP⁺ cells were counted in each mouse; statistical significance was determined using χ^2 test: $\chi^2(15) = 969.17$, $P < 0.00001$). (**F**–**H**) *Krt15-CrePR1 R26*^{Conf} mice were injected every 12 hours with 1 mg of RU486 for 10 consecutive days and sacrificed 2 months later. (**G**) Whole-mount esophageal image of *Krt15-CrePR1 R26*^{Conf} mice sacrificed 2 months after recombination. (**H**) Representative example of a monochromatic clonal unit in a transverse esophageal section. Dotted line marks the basement membrane. Scale bars: 50 μm.

strate the persistence of *Krt15*-labeled cells in the esophageal epithelium well beyond the homeostatic renewal time of the mouse esophagus of 7–10 days and support the premise of the existence of a long-lived subpopulation of basal cells.

Krt15-derived cells organize as clonal units. Classic studies have demonstrated that mitosis occurs in the basal layer, whereas early differentiation commences in the suprabasal layer, and terminal differentiation in the superficial squamous layer concomitant

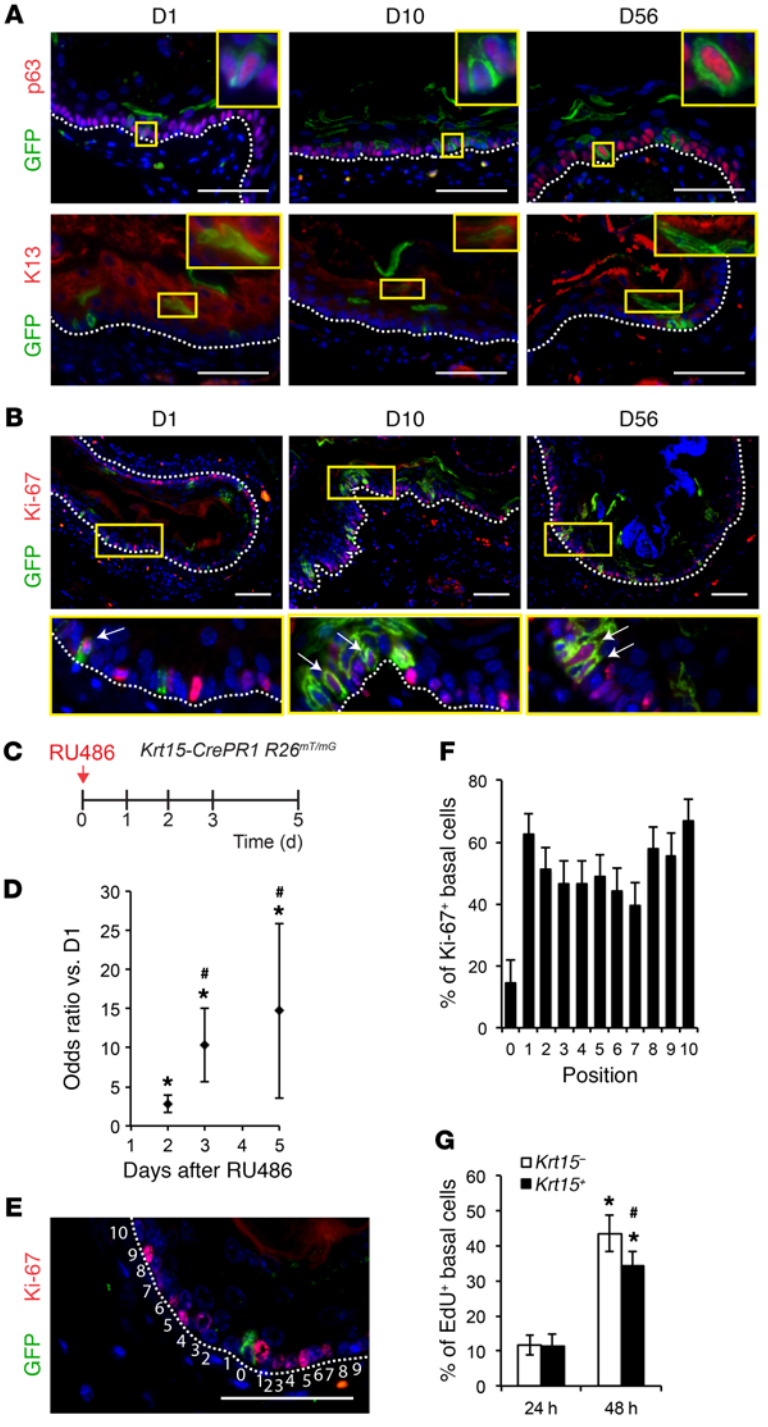

Figure 3. Basal *Krt15*⁺ cells give rise to all squamous lineages in the esophageal epithelium. (**A** and **B**) *Krt15-CrePR1 R26*$^{mT/mG}$ mice were injected daily with 0.5 mg RU486 for 5 consecutive days and sacrificed at listed time points. (**A**) Colocalization of *Krt15*⁺ (GFP) cells with p63 (basal cell marker) and K13 (suprabasal cell marker). Magnifications of regions of interest are displayed in a yellow rectangle. (**B**) Colocalization of *Krt15*⁺ (GFP) cells with Ki-67. Magnifications of regions of interest are displayed in a yellow rectangle. Arrows indicate colocalization events. (**C** and **D**) *Krt15-CrePR1 R26*$^{mT/mG}$ mice were injected once with 0.5 mg RU486 and sacrificed 1, 2, 3, and 5 days after. (**D**) The percentage of Ki-67⁺/GFP⁺ basal cells was determined. Graph represents mean odds ratios ± SEM versus D1 (n = 2–4 mice at each time point; cross sections of 4 different regions of the esophagus were analyzed for each mouse). $^{*}P \le 0.05$ vs. D1 and $^{\#}P \le 0.05$ vs. D2 using z test. (**E** and **F**) *Krt15-CrePR1 R26*$^{mT/mG}$ mice were injected once with 0.5 mg RU486 and sacrificed 1 day after. The percentage of Ki-67⁺ cells at each position surrounding the GFP (*Krt15*⁺) cells (position 0) was determined. Graph represents mean ± SEM (n = 4 mice; cross sections of 4 different regions of the esophagus were analyzed for each mouse); probability of having Ki-67⁺ cells in position 1 to 10 vs. position 0 was determined using χ^2 test: $\chi^2(10) = 20.44$, $P = 0.025$. (**G**) *Krt15-CrePR1 R26*$^{mT/mG}$ mice were injected once with 0.5 mg RU486 and sacrificed 24 or 48 hours after. Mice were also injected with EdU 1.5 hours before sacrifice. Percentage of EdU⁺ cells among *Krt15*⁻ and *Krt15*⁺ basal cells was determined by flow cytometry. Graph represents mean ± SEM (n = 4 mice per group, $^{*}P < 0.05$ [48 vs. 24 hours] and $^{\#}P < 0.05$ [*Krt15*⁺ vs. *Krt15*⁻], using Wald χ^2 test). Dotted line marks the basement membrane. Scale bars: 50 μm.

with migration of cells from the basal layer to the luminal surface (13, 29). In our study, clonal units derived from *Krt15*-labeled cells were observed 7 days after recombination (Figure 2A). These units mostly form a cohesive cell cluster suggesting expansion from an original *Krt15*⁺ cell with little lateral cell migration under homeostatic conditions. Imaging of thick esophageal tissue sections using confocal microscopy reinforces the clustered nature of *Krt15*-derived clonal units (Figure 2B and Supplemental Video 1). 3D reconstruction was used to illustrate the clustering of *Krt15*⁺ clonal units. Basal cells were labeled in blue tones and suprabasal cells in red tones. The reconstruction suggests that the original *Krt15*⁺ cells divide to give rise to multiple basal cells (blue tones) and cells emerging in the suprabasal layer (yellow cell in Figure 2, C and D, and Supplemental Video 2). These differentiated cells then migrate toward the luminal surface while remaining clustered. Interestingly, we observed occasionally a single GFP⁺ cell in the basal layer with no neighboring parabasal or suprabasal GFP⁺ cells (white cell in Figure 2, C and D, and Supplemental Video 2), suggesting that not all *Krt15*⁺ cells are always actively dividing. Epithelial homeostasis is maintained presumably by a balanced

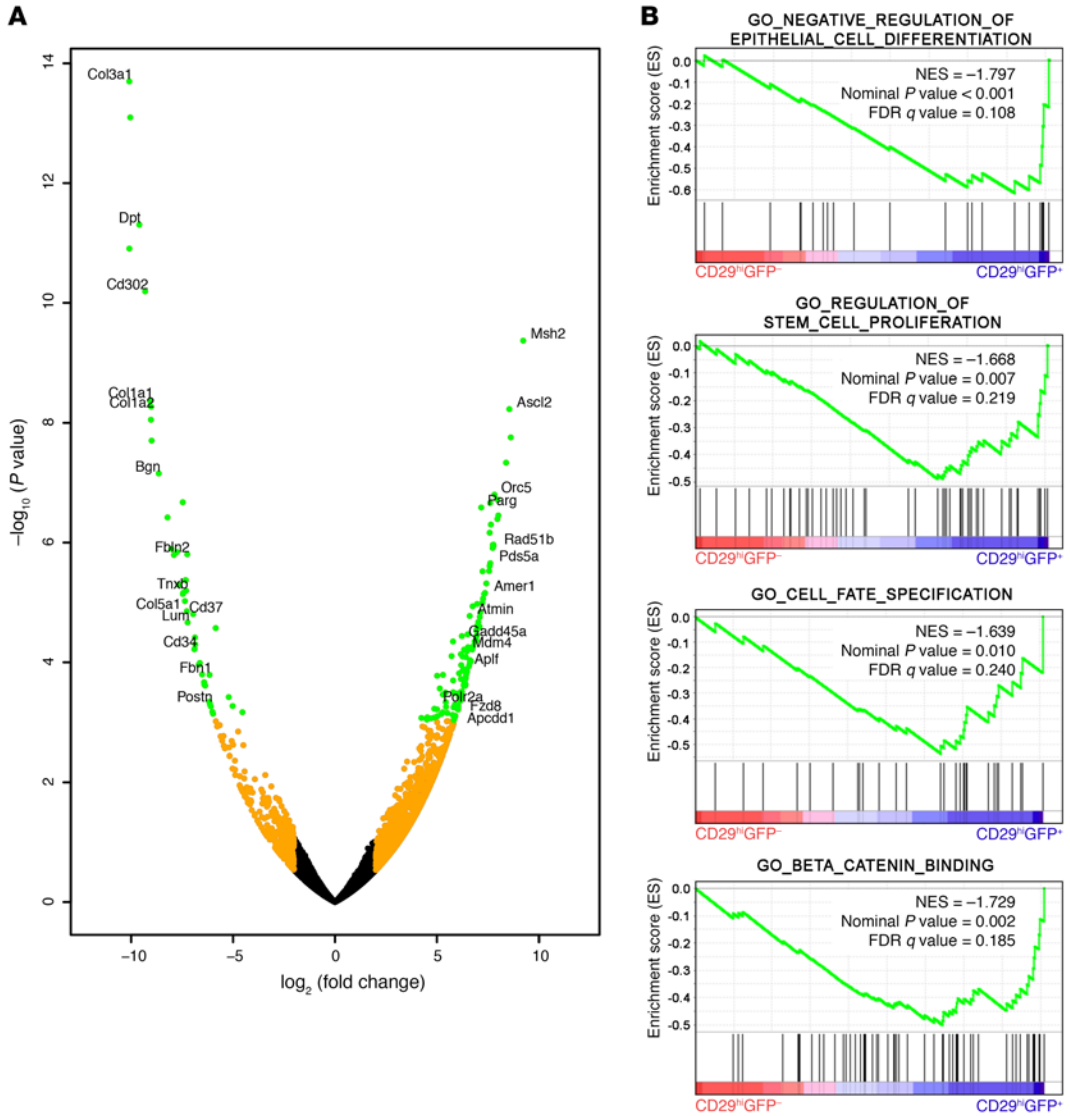

Figure 4. *Krt15*⁺ basal cells have a distinct transcriptional profile compared with *Krt15*⁻ basal cells. (**A** and **B**) *Krt15-CrePR1 R26*$^{mT/mG}$ mice were injected once with 0.5 mg RU486 and sacrificed 24 hours later. *Krt15*⁺ basal cells (CD29^{hi}GFP⁺) and *Krt15*⁻ basal cells (CD29^{hi}GFP⁻) were sorted and subjected to RNA-Seq (n = 3). (**A**) Volcano plot representation of up- and downregulated genes in *Krt15*⁺ basal cells versus *Krt15*⁻ basal cells as measured by RNA-Seq. Green dots represent significantly regulated genes ($\log_2$ fold change > 2 and adjusted $P < 0.05$). (**B**) GSEA of *Krt15*⁺ and *Krt15*⁻ basal cells. Representative plots of some of the significantly enriched gene sets in *Krt15*⁺ basal cells (false discovery rate < 0.25 and $P < 0.05$). NES, normalized enrichment score.

number of proliferation, differentiation, migration, and apoptotic events. Between D1–D3 and D3–D5 following recombination, we observed a significant decrease in the basal cell/parabasal cell ratio concomitant with an increase in the number of suprabasal cells. This is in line with the time necessary for basal cell division and migration to the suprabasal layer (Figure 2E). Beyond 5 days after recombination, the proportion of GFP⁺ cells in the different layers remained constant through time, suggesting that the equilibrium of *Krt15*⁺ clones was preserved (Figure 2E). Furthermore, clone numbers were quantified at different time points following the last RU486 injection to assess *Krt15*⁺-derived clone maintenance, and we determined that approximately 15% of the original *Krt15*⁺ clones were maintained up to 6 months following RU486 treatment (Supplemental Figure 3B).

The *R26*$^{mT/mG}$ reporter does not allow discrimination between clones that originated from 1 versus multiple *Krt15*⁺ cells. Therefore, to assess the capacity of a single *Krt15*⁺ cell to give rise to a clonal unit, we used the 4-color Confetti reporter mouse (*R26*^{Conf}) (Figure 2F) (26). *Krt15-CrePR1 R26*^{Conf} mice were treated with RU486 and sacrificed 2 months later. All clones visualized using a dissection scope appeared to be monochromatic (Figure 2G). Imaging of transverse esophagus sections confirmed the monochromaticity of *Krt15*-derived clonal units (Figure 2H). When 2 clones were found close together, cell clusters were not intermixed, supporting the possibility of monoclonal expansion of *Krt15*⁺ clones (Supplemental Figure 3C). These results suggest that clonal units derived from *Krt15*⁺ cells originate from a single recombination event. However, because of the low Cre recombi-

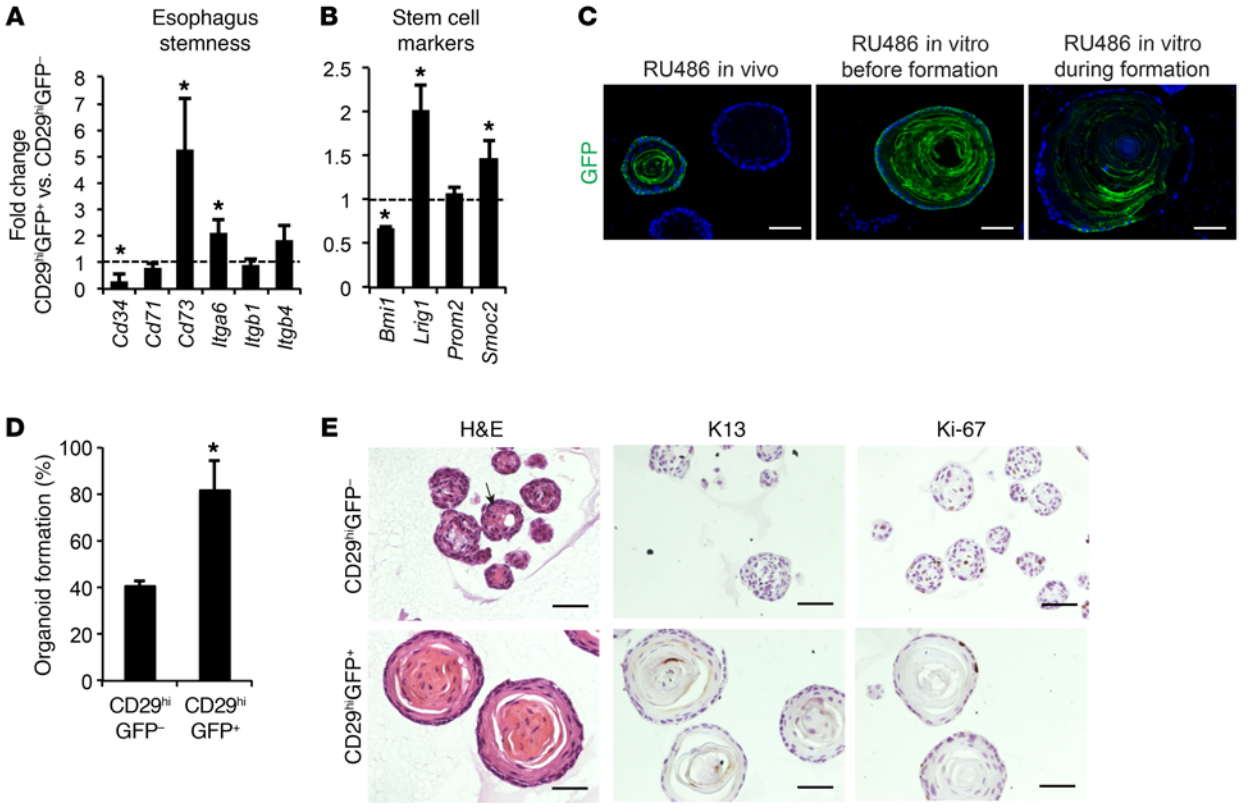

Figure 5. *Krt15*⁺ basal cells have a higher clonogenic potential than *Krt15*⁻ basal cells. (**A** and **B**) *Krt15-CrePR1 R26*$^{mT/mG}$ mice were injected once with 0.5 mg RU486 and sacrificed 24 hours later. *Krt15*⁺ basal cells (CD29^{hi}GFP⁺) and *Krt15*⁻ basal cells (CD29^{hi}GFP⁻) were sorted and analyzed. Expression of genes related to esophageal epithelium stemness (**A**) and some tissue epithelial stem cell genes (**B**) was quantified by quantitative PCR. Graphs represent mean ± SEM (n = 3–7 mice for each population, *$P \leq 0.05$ using 2-tailed Student's t test). (**C**) 3D organoids were established from *Krt15-CrePR1 R26*$^{mT/mG}$ mice. Cre recombination was induced by RU486 treatment in vivo (left panel), in vitro when the 3D organoids were seeded (middle panel), or in vitro after 3D organoid formation (right panel). *Krt15*-derived cells were visualized with GFP immunofluorescence. (**D** and **E**) *Krt15-CrePR1 R26*$^{mT/mG}$ mice were injected with a single dose of RU486 and sacrificed 24 hours later. *Krt15*⁺ basal cells (CD29^{hi}GFP⁺) and *Krt15*⁻ basal cells (CD29^{hi}GFP⁻) were sorted and seeded in Matrigel. (**D**) 3D organoid formation rate was assessed in 4 different mice and repeated at different passages. Graph represents mean ± SEM of a representative experiment executed in quadruplicate fashion; *$P \leq 0.05$ using 2-tailed Student's t test. (**E**) CD29^{hi}GFP⁻ and CD29^{hi}GFP⁺ cell–derived 3D organoids were stained with H&E, Ki-67 (proliferative cells), and K13 (suprabasal cells). Arrow indicates rare keratin hyaline granules. Scale bars: 50 μm.

nation rate in this model, we cannot exclude the possibility of 2 or more *Krt15*⁺ basal cells expanding as a cohesive clonal unit in a model with a higher recombination rate such as *R26*$^{mT/mG}$.

Krt15⁺ *basal cells give rise to all differentiated lineages in the esophageal epithelium.* A critical property of a somatic stem/progenitor cell is the capacity to give rise to all the lineages within the tissue in which it resides. Therefore, we costained esophageal tissues from *Krt15-CrePR1 R26*$^{mT/mG}$ mice harvested 1, 10, and 56 days after Cre recombination with markers of basal and suprabasal cells. We observed that *Krt15*⁺ basal cells expand to give rise to p63⁺ basal cells and K13⁺ suprabasal cells (Figure 3A). Proliferative basal cells (Ki-67⁺) can also originate from *Krt15*⁺ basal cells (Figure 3B). To determine the proliferation rate of *Krt15*⁺ cells over time, we induced Cre recombination in *Krt15-CrePR1 R26*$^{mT/mG}$ mice with a single dose of RU486 and sacrificed the mice 1, 2, 3, or 5 days after recombination (Figure 3C). Twenty-four hours after recombination, we observed that the probability of observing Ki-67 positivity in *Krt15*-derived (GFP⁺) cells was 2.8 times greater at D2 (P = 0.0075), 10.34 at D3 (P < 0.0001), and 14.7 at D5 versus D1 (P = 0.0004) (Figure 3D). The Wald χ^2 test also demonstrated statistical differences between the percentages of Ki-67⁺/GFP⁺ basal cells at each time point [$\chi^2(3) = 31.81$, $P = 5.73 \times 10^{-7}$]. We also analyzed the probability of observing Ki-67⁺ cells contiguous and adjacent to *Krt15*-derived cells (position 0) (Figure 3, E and F). We observed that the percentage of Ki-67⁺ cells in positions 1–10 was 6.4 times higher than the percentage in position 0 [$\chi^2(10) = 20.44$, $P = 0.025$], but the percentages of Ki-67⁺ cells were not different between positions 1 and 10 (Figure 3F). We also determined the percentage of *Krt15*⁺ basal cells in S phase of the cell cycle at different time points using 5-Ethynyl-2′-deoxyuridine (EdU) incorporation assay (Figure 3G). The percentage of EdU⁺ cells in the *Krt15*-derived cell population was higher 48 hours following Cre induction versus 24 hours, confirming the result presented in Figure 3D. Furthermore, the percentage of EdU⁺ cells among *Krt15*⁺ basal cells was lower than that among *Krt15*⁻ basal cells at 48 hours following Cre induction (Figure 3G). These results suggest that *Krt15*⁺ basal cells are less proliferative than their neighboring cells, supporting their distinctive nature.

Krt15⁺ *basal cells are transcriptionally distinct from Krt15*⁻ *basal cells.* Heterogeneity within the basal cell layer has been suggested (11) with ITGA6^{hi}ITGB4^{hi}CD73⁺ cells having a higher 3D organoid

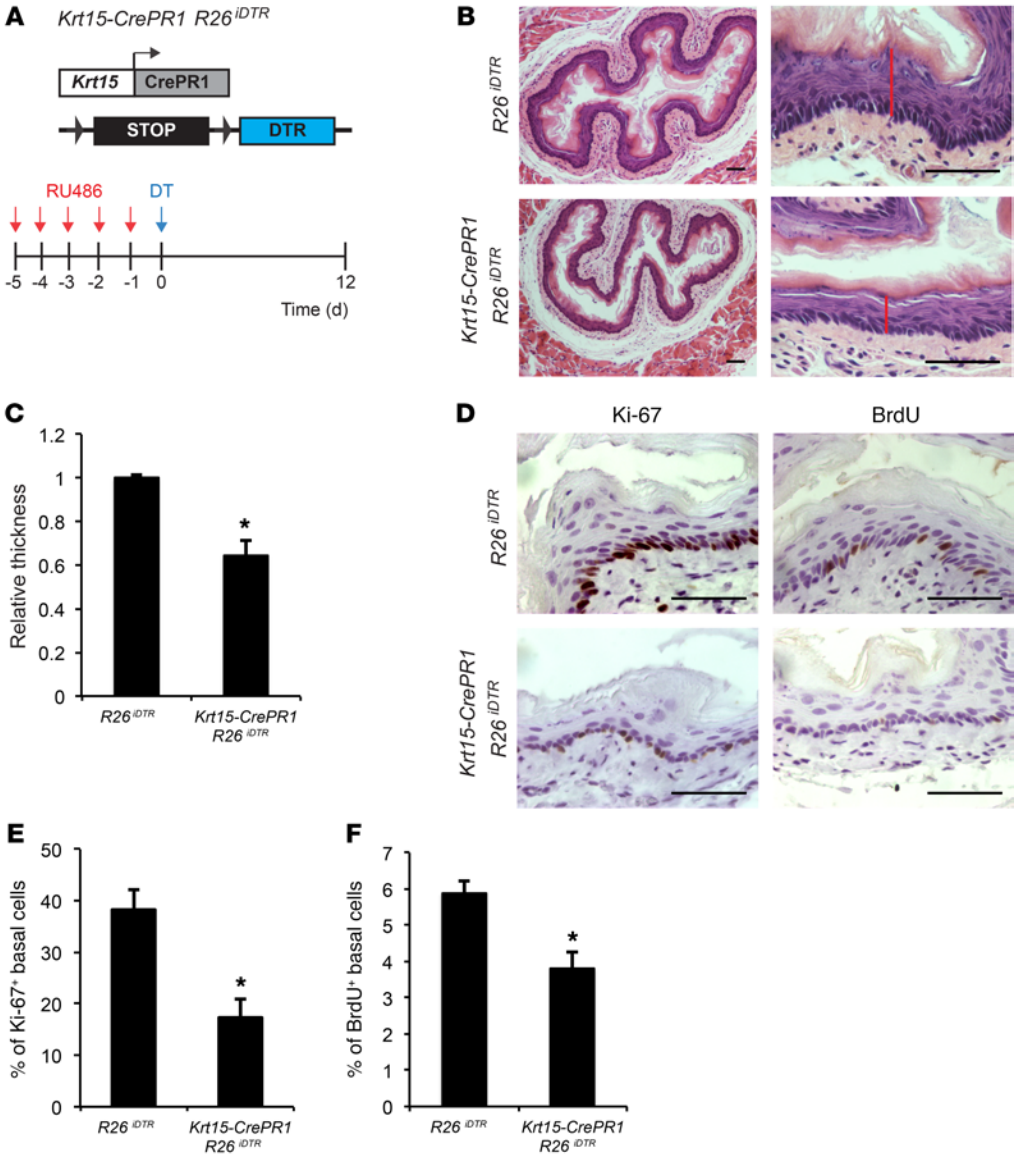

Figure 6. Depletion of *Krt15*⁺ cells leads to reduced proliferation and epithelial atrophy. (**A**–**F**) *Krt15-CrePR1 R26*^{iDTR} and control (*R26*^{iDTR}) mice were injected daily with 0.5 mg RU486 for 5 consecutive days prior to diphtheria toxin (DT) injection to deplete *Krt15*-derived cells. Mice were sacrificed 12 days after DT administration or sooner in case of extensive weight loss. (**B**) H&E of the esophagi of *Krt15-CrePR1 R26*^{iDTR} mice and age-matched *R26*^{iDTR} control mice. Red lines delineate epithelial thickness. (**C**) Epithelial thickness was measured at 4 representative spots of 4 different cross-sectional regions of each esophagus (n = 5 mice per group). Graph represents mean ± SEM; *$P \leq 0.05$ using 2-tailed Student's t test. (**D**–**F**) *Krt15-CrePR1 R26*^{iDTR} and control *R26*^{iDTR} mice were injected with BrdU 1.5 hours before sacrifice, and esophageal sections were stained for Ki-67 and BrdU. The percentage of Ki-67⁺ (**E**) and BrdU⁺ (**F**) basal cells was determined. Graphs represent mean ± SEM (n = 5 mice per group, and a minimum of 500 basal cells was counted; *$P \leq 0.05$ using 2-tailed Student's t test). Scale bars: 50 μm.

formation capacity within the basal cell subpopulations examined. Therefore, to determine whether *Krt15*⁺ basal cells are distinct from the other basal cells, we isolated *Krt15*⁺ basal cells from *Krt15-CrePR1 R26*$^{mT/mG}$ mice 24 hours after recombination, before division of lineage-labeled cells. In our experiments, we used the basal marker CD29 (integrin β_1, *Itgb1*) to isolate basal cells as described previously (10, 11). Specificity of CD29 expression in basal cells was confirmed by immunostaining (Supplemental Figure 4A). CD29^{hi}GFP⁺ (*Krt15*⁺) and CD29^{hi}GFP⁻ (*Krt15*⁻) basal cells were sorted from esophageal epithelial single-cell suspensions (Supplemental Figure 4B). RNA-Seq was performed on both populations, and we identified 116 upregulated and 48 downregulated genes in *Krt15*⁺ basal cells versus *Krt15*⁻ basal cells (Figure 4A and Supplemental Table 1). GSEA was performed and revealed enrichment for gene sets correlating with negative regulation of epithelial differentiation, regulation of stem cell proliferation, and cell fate specification in *Krt15*⁺ basal cells (Figure 4B). A distinct Wnt signaling signature between *Krt15*⁺ and *Krt15*⁻ basal cells was suggested from the RNA-Seq data. GSEA suggested enrichment for the β-catenin binding gene set in *Krt15*⁺ basal cells (Figure 4B). Interestingly, *Ascl2* was the third most upregulated gene in *Krt15*⁺ basal cells (375-fold, $P = 3.13 \times 10^{-5}$), a known Wnt signaling gene target associated with stemness in intestinal epithelium (30). We also noted an increase of other Wnt signaling–associated

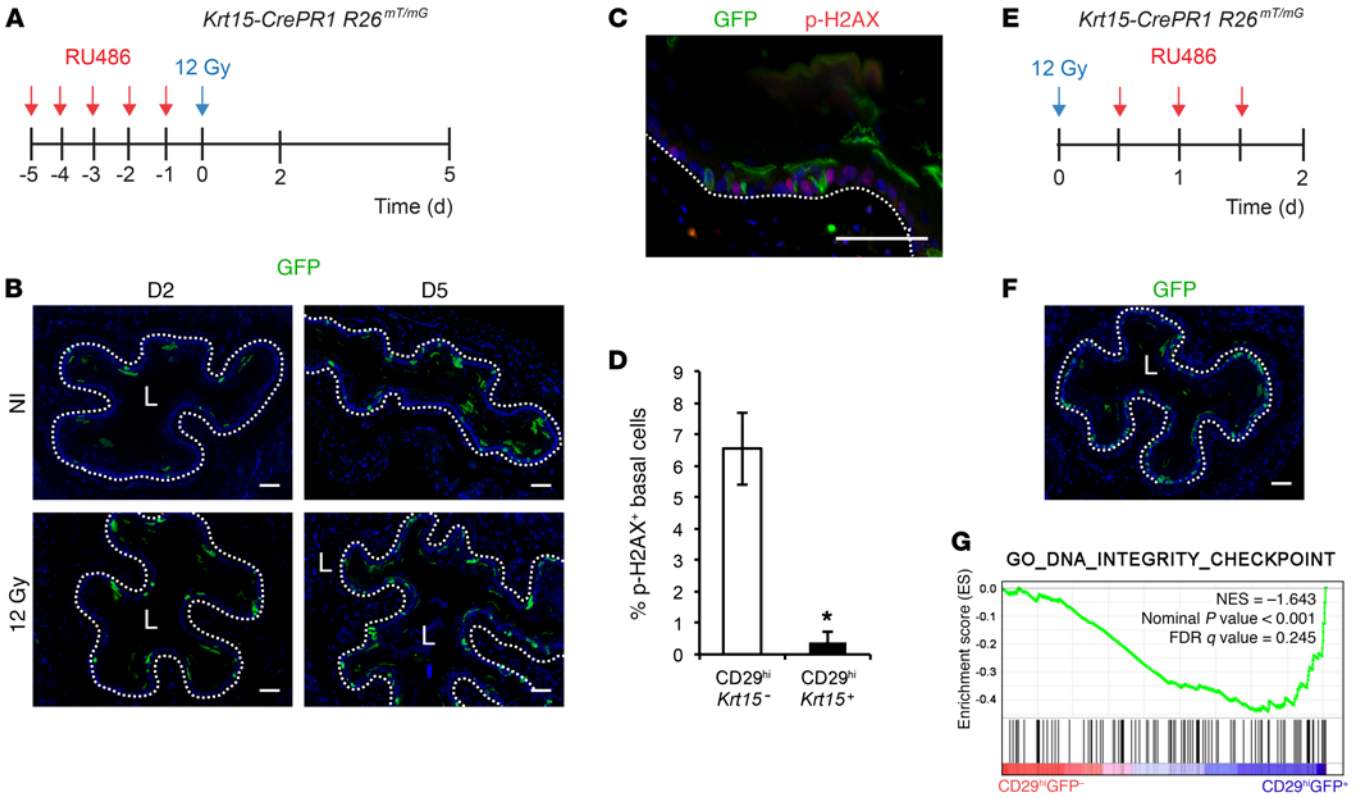

Figure 7. *Krt15*⁺ cells are radioresistant to high-dose radiation. (**A**–**D**) *Krt15-CrePR1 R26*$^{mT/mG}$ mice were injected daily with 0.5 mg RU486 for 5 consecutive days. Fifty percent of mice were subjected to 12 Gy whole-body irradiation on the following day, and sacrificed 2 or 5 days after radiation. (**B**) *Krt15*-derived cells were visualized by GFP immunofluorescence in the esophagi of *Krt15-CrePR1 R26*$^{mT/mG}$ mice that were irradiated or not irradiated (NI). (**C** and **D**) p-H2AX and GFP (*Krt15*-derived cells) immunofluorescence was performed of esophagi harvested from the mice sacrificed 2 days after irradiation. (**D**) Percentage of p-H2AX⁺ staining in *Krt15*⁻ and *Krt15*⁺ basal cells was quantified. Graph represents mean ± SEM (n = 3 mice; cross sections of 4 different regions of the esophagus were analyzed for each mouse); *$P \leq 0.05$ using 2-tailed Student's t test. (**E** and **F**) *Krt15-CrePR1 R26*$^{mT/mG}$ mice were subjected to 12 Gy whole-body irradiation and then injected every 12 hours with RU486 until sacrifice 48 hours after irradiation. (**F**) *Krt15*-derived cells were visualized by GFP immunofluorescence in the esophagi of *Krt15-CrePR1 R26*$^{mT/mG}$ mice. (**G**) *Krt15-CrePR1 R26*$^{mT/mG}$ mice were injected once with 0.5 mg RU486 and sacrificed 24 hours later. *Krt15*⁺ basal cells (CD29^{hi}GFP⁺) and *Krt15*⁻ basal cells (CD29^{hi}GFP⁻) were sorted and subjected to RNA-Seq. GSEA was performed in *Krt15*⁺ and *Krt15*⁻ basal cells. Plot of DNA integrity checkpoint gene set enriched in *Krt15*⁺ basal cells (false discovery rate < 0.25 and $P < 0.05$). "L" indicates the lumen; dotted line marks the basement membrane. Scale bars: 50 μm.

genes such as *Amer1*, *Fzd8*, and *Apcdd1* (Figure 4A and Supplemental Table 1). By contrast, *Krt15*⁻ basal cells were enriched for extracellular matrix structural constituent and ribosome gene sets (Supplemental Figure 4C). Indeed, downregulated genes in *Krt15*⁺ basal cells encode for proteins associated with extracellular matrix such as collagens, periostin, and proteoglycans (Figure 4A and Supplemental Table 2).

Using a more targeted approach, we also determined the expression of several membrane proteins that have been associated previously with esophageal epithelial stemness potential (9, 11, 12, 31). *Krt15*⁺ cells exhibit reduced expression of *Cd34*, a previously identified marker of a label-retaining subpopulation of basal cells (Figure 5A), thereby suggesting that *Krt15*⁺ and CD34⁺ populations are distinct (12). Interestingly, RNA-Seq identified *Cd34* as a downregulated gene in *Krt15*⁺ basal cells (Figure 4A and Supplemental Table 2). Increased expression of *Itga6* and *Cd73* was also observed in *Krt15*⁺ basal cells (Figure 5A). Notably, ITGA6^{hi}ITGB4^{hi}CD73⁺ cells have the highest 3D organoid formation capacity of the examined cell populations (11). Expression of certain epithelial stem cell genes in other tissues was measured (Figure 5B). Interestingly, we observed a significant decrease in the oncogene *Bmi1* and an increase in *Lrig1* and *Smoc2* expression in *Krt15*⁺ basal cells versus *Krt15*⁻ basal cells. All together, these results suggest distinct transcriptional profiles of *Krt15*⁺ and *Krt15*⁻ basal cells, supporting the premise of heterogeneity within the esophageal basal layer.

Krt15⁺ *cells give rise to fully differentiated 3D organoids.* To elaborate on the distinctive properties of *Krt15*⁺ basal cells, we used 3D organoid culture to assess clonogenicity. 3D organoids formed with cells isolated from *Krt15-CrePR1 R26*$^{mT/mG}$ mice following in vivo Cre recombination were either entirely GFP⁺ or entirely GFP⁻, suggesting that 3D organoids arise clonally in this culture model (Figure 5C, left panel). In vitro Cre recombination immediately after seeding also resulted in formation of organoids that were entirely GFP⁺ or GFP⁻ (Figure 5C, middle panel). Finally, Cre recombination following organoid establishment demonstrated that *Krt15*⁺ cells exist in 3D organoids and give rise to clonal units (Figure 5C, right panel). To compare the clonogenic potential of *Krt15*⁺ and *Krt15*⁻ basal cells, we plated CD29^{hi}GFP⁻ (Tomato⁺) and CD29^{hi}GFP⁺ (GFP⁺) cells sorted from

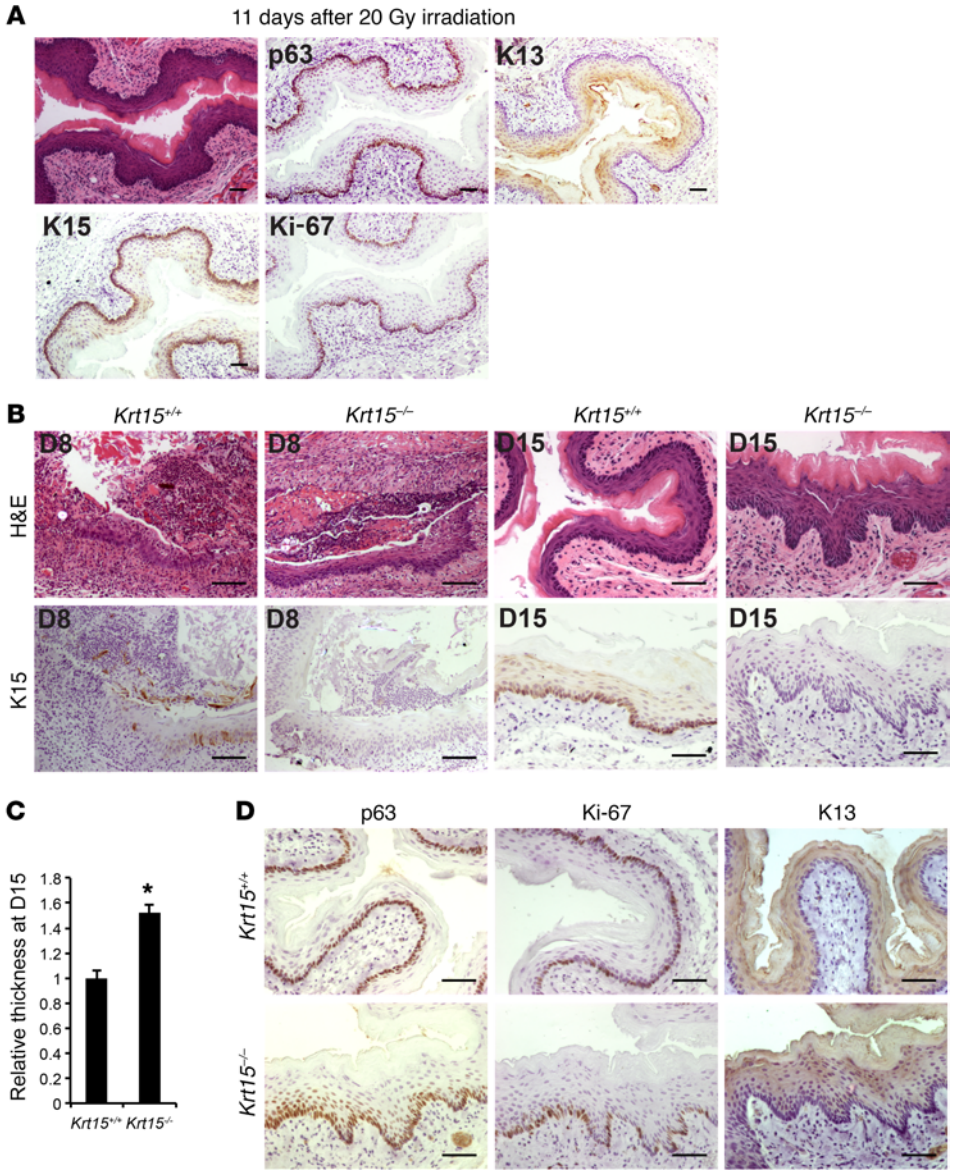

Figure 8. *Krt15* deficiency impairs tissue regeneration following high-dose radiation. (**A**) Esophagi of C57BL/6J WT mice were locally irradiated with 20 Gy, and mice were sacrificed 11 days after irradiation. H&E staining and immunohistochemistry of K15, K13, p63, and Ki-67 were performed. (**B**–**D**) *Krt15*$^{+/+}$ and *Krt15*$^{-/-}$ mice were subjected to esophageal-targeted 20-Gy irradiation and sacrificed 8 and 15 days after radiation. (**B**) H&E staining and K15 immunohistochemistry of esophagi locally irradiated with 20 Gy from *Krt15*$^{+/+}$ and *Krt15*$^{-/-}$ mice. (**C**) Epithelial thickness was measured 15 days after esophageal-targeted irradiation. Four representative measurements of 2 different cross-section regions of each esophagus were done (n = 2–3 mice per group). Graph represents mean ± SEM; *$P \leq 0.05$ using 2-tailed Student's t test. (**D**) Immunohistochemistry of p63, K13, and Ki-67 in the esophagi locally irradiated with 20 Gy. Scale bars: 50 μm.

Krt15-CrePR1 R26$^{mT/mG}$ mice (Supplemental Figure 4D) and measured the 3D organoid formation rate of both cell populations. *Krt15*$^{+}$ basal cells formed more 3D organoids than *Krt15*$^{-}$ basal cells, indicating that *Krt15*$^{+}$ cells are more clonogenic (Figure 5D). Interestingly, CD29^{hi}GFP^{-} and CD29^{hi}GFP^{+} cells generated 3D organoids with marked histological differences (Figure 5E). *Krt15*$^{+}$-derived organoids are larger and exhibit differentiation with a keratinized center showing a gradual, normal differentiation pattern. *Krt15*$^{-}$ basal cells formed smaller, more cellular 3D organoids with little keratinization. Although rare, cells containing keratin granules could be observed especially in the center of 3D organoids derived from *Krt15*$^{-}$ cells (Figure 5E, arrow). This abrupt keratinization suggests that the *Krt15*$^{-}$ cells can become terminally differentiated without transitioning through intermediate morphological steps such as cell elongation. In contrast to *Krt15*$^{-}$ cells, *Krt15*$^{+}$ cells formed differentiated 3D organoids as observed by K13^{+} expression in the inner layers (Figure 5E). Furthermore, Ki-67 staining confirmed that proliferation was restricted to the outer cell layer as expected in *Krt15*$^{+}$-derived 3D organoids, whereas Ki-67^{+} cells could be observed throughout the *Krt15*$^{-}$-derived 3D organoids. These results suggest that unlike *Krt15*$^{-}$ basal cells, *Krt15*$^{+}$ basal cells can recapitulate esophageal epithelial homeostasis in 3D organoids, supporting their clonogenicity and multipotency.

Depletion of Krt15⁺ cells results in diminished proliferation and epithelial atrophy. Our results thus far demonstrate that *Krt15*⁺ basal cells are sufficient to undergo proliferative expansion and give rise to all states of lineage commitment in the mouse esophageal epithelium and have higher clonogenic potential than *Krt15*⁻ basal cells. We next investigated the necessity of *Krt15*⁺ cells for esophageal function in vivo. We ablated *Krt15*-derived cells in the adult mouse using an inducible diphtheria toxin receptor (iDTR) system (32) and analyzed the morphology of the esophageal epithelium. *Krt15-CrePR1 R26*^{iDTR} mice were injected with RU486 for 5 consecutive days followed by diphtheria toxin administration (Figure 6A). Mice were then sacrificed 12 days after *Krt15*⁺ cell depletion or before excessive weight loss. Morphological analysis of the esophagi revealed a significant diminution in the stratification (thinning) of the esophageal epithelium in *Krt15-CrePR1 R26*^{iDTR} mice in comparison with control mice (*R26*^{iDTR}) (Figure 6, B and C). We quantified the proliferation of basal cells in both cohorts to determine whether epithelial thinning was the result of decreased proliferation. The percentage of Ki-67⁺ cells in the basal layer was reduced significantly in *Krt15-CrePR1 R26*^{iDTR} mice (Figure 6, D and E). BrdU incorporation was also decreased in *Krt15-CrePR1 R26*^{iDTR} mice (Figure 6, D and F). Thus, *Krt15*-derived cells are important for maintaining the proliferative output necessary for normal esophageal homeostasis.

Krt15⁺ cells are radioresistant and facilitate tissue regeneration following high-dose irradiation. Epithelial stem cells participate actively in tissue regeneration in response to injury such as irradiation (3). Since *Krt15*⁺ cells present characteristics consistent with long-lived progenitor cells in the mouse esophagus, we studied their role in response to radiation-induced injury. First, C57BL/6J WT mice were subjected to 12 Gy whole-body γ-irradiation and sacrificed at different time points (4 hours to 7 days). Signs of DNA damage were observed in the esophageal epithelium 4 hours after irradiation, including increased p-H2AX staining (Supplemental Figure 5A). Also, clusters of Ki-67⁺ proliferative cells were observed 5 days after irradiation, suggesting that activation of basal cells contributes to regeneration of the injured tissue. Although morphology was only modestly affected in the esophagus, induction of K15 expression was observed in suprabasal cells, suggesting a possible role for K15 protein itself in esophageal epithelial regeneration (Supplemental Figure 5, A and B). Interestingly, *Krt15* mRNA expression (but not expression of other epithelial stem cell markers) was increased in organoids following irradiation, confirming the specific induction of *Krt15* in response to injury (Supplemental Figure 5C). In the small intestine, the active Wnt^{hi} *Lgr5*⁺ stem cell population is sensitive to high-dose irradiation, whereas a Wnt$^{lo/off}$ reserve stem cell population is radioresistant and can give rise to active *Lgr5*⁺ stem cells following damage (33, 34). Furthermore, we have reported recently that *Krt19*⁺ intestinal stem cells expand after radiation-induced injury through lineage labeling (35). Therefore, we investigated whether *Krt15*⁺ cells are resistant to high-dose irradiation by irradiating *Krt15-CrePR1 R26*$^{mT/mG}$ mice (Figure 7A). Cre recombination was induced prior to irradiation, and we noted that GFP⁺ (*Krt15*⁺) cells persisted for 5 days following irradiation, suggesting that *Krt15*⁺ cells are radioresistant in the esophageal epithelium (Figure 7B). We also observed that the percentage of p-H2AX⁺ cells was higher in the *Krt15*⁻ basal cells versus the *Krt15*⁺ basal cells, suggesting a unique radioresistance in *Krt15*⁺ basal cells (Figure 7, C and D). Furthermore, when Cre recombination was induced following irradiation in *Krt15-CrePR1 R26*$^{mT/mG}$ mice, *Krt15*⁺ cells were able to undergo lineage tracing and expansion, giving rise to clonal units (Figure 7, E and F). These results suggest that *Krt15*⁺ basal cells are less susceptible to high-dose radiation and could therefore be active in the regeneration process.

Interestingly, GSEA indicates an enrichment for DNA integrity checkpoint gene set in *Krt15*⁺ versus *Krt15*⁻ basal cells (Figure 7G). Furthermore, the most upregulated gene in *Krt15*⁺ basal cells was *Msh2* (600-fold versus *Krt15*⁻ basal cells), a key regulator of DNA mismatch repair (MMR) that has been associated with microsatellite instability in several solid tumors. Stem or progenitor cells have been reported to display higher MMR activity to assure DNA integrity throughout their rapid proliferation (36, 37). We also observed increase of several DNA damage response–associated genes, such as *Rad51b*, *Parg*, *Atmin*, *Aplf*, *Mdm4*, and *Gadd45a* (Figure 4A and Supplemental Table 1). These results suggest a possible role for these genes in *Krt15*⁺ cells in response to injury-induced DNA damage.

Since whole-body irradiation induces damage to the bone marrow and intestinal epithelium, requiring early sacrifice, we used esophageal-targeted high-dose irradiation to further study esophageal epithelial regeneration. First, C57BL/6J WT mice were imaged with a CT scan to visualize the trachea as an anatomic landmark to target irradiation to the esophagus (Supplemental Figure 6A). Pilot experiments demonstrated that 20 Gy esophagus-targeted irradiation was sufficient to induce morphological changes and weight loss (Supplemental Figure 6, B and C). In the recovery period (D11), we noted epithelial thickening and epithelial downgrowth (indentation), suggesting that the esophageal epithelium was actively recovering from the radiation insult. Basal cell hyperplasia was also observed, as illustrated by the presence of more than one p63⁺ basal cell layer. Furthermore, proliferative cells were not restricted to the basal layer (Figure 8A).

To investigate in a complementary fashion a possible functional role of the K15 protein in response to irradiation, we irradiated the esophagi of *Krt15*$^{+/+}$ and *Krt15*$^{-/-}$ mice and sacrificed the animals 8 days and 15 days after irradiation. D8 was chosen as a representative time point for maximal tissue injury and D15 as the recovery time point when tissue regeneration is complete. At D8, epithelial damage was similar between *Krt15*$^{+/+}$ and *Krt15*$^{-/-}$ mice. Acute ulcerative esophagitis was observed with some residual epithelial cells still present (Figure 8B). At D15, the esophagi of *Krt15*$^{+/+}$ mice had a normal morphology. Interestingly, basal cell hyperplasia and epithelial downgrowth, which are distinctive features of injured tissue, were still present in the esophagi of *Krt15*$^{-/-}$ mice, suggesting that K15 loss impaired complete tissue regeneration (Figure 8B). The esophageal epithelia of *Krt15*$^{-/-}$ mice were 50% thicker than their counterparts from *Krt15*$^{+/+}$ mice at D15 (Figure 8C). *Krt15*$^{-/-}$ mice revealed more p63⁺ basal cell layers, underscoring the basal cell hyperplasia phenotype. Proliferative cells could also be observed in cell layers closer to the lumen in *Krt15*$^{-/-}$ mice, suggesting that the esophagus was still recovering from the high-dose radiation. Differentiation was also altered in

Krt15$^{-/-}$ mice compared with *Krt15*$^{+/+}$ mice as illustrated by changes in K13 expression (Figure 8D). Finally, 3D organoids grown from irradiated *Krt15*$^{+/+}$ and *Krt15*$^{-/-}$ mice sacrificed at D15 recapitulated the changes observed in these mice (Supplemental Figure 6D). Esophageal epithelial cells isolated from a *Krt15*$^{+/+}$ mouse formed normal 3D organoids, i.e., almost perfect spheres with a smooth perimeter. Conversely, organoids formed from *Krt15*$^{-/-}$ esophageal cells were hypertrophic and irregular in shape. Foci of cellular crowding could be observed mostly in the basaloid layer, consistent with basal cell hyperplasia. Also, *Krt15*$^{-/-}$-derived 3D organoids had abundant central keratin mass characterized by nuclear retention in the keratinized cells (parakeratinization), a sign of rapid turnover from basal to surface cells. Altogether, these results suggest that *Krt15*$^{+}$ cells are radioresistant to high-dose radiation and contribute to tissue regeneration. Furthermore, and as a separate consideration, *Krt15* deficiency impairs tissue regeneration in response to radiation-induced injury.

Discussion

The rapid renewal of the esophageal epithelium is maintained by highly proliferative basal cells; the involvement of a subpopulation of basal cells with properties consistent with stem cells or long-lived progenitor cells remains to be fully demonstrated. Here, we show that the *Krt15* promoter marks a long-lived (>6 months) basal cell subpopulation that gives rise to all differentiated lineages in the esophageal epithelium, representing, to our knowledge, the first genetic in vivo lineage tracing evidence of such a progenitor cell population. We demonstrate that *Krt15*$^{+}$ basal cells display increased 3D organoid formation capacity and *Krt15*-derived 3D organoids are more differentiated, suggesting greater self-renewal and multipotency as independent corroboration of the in vivo findings.

Stem and progenitor cells participate in the regenerative response to injury in different tissues. An esophageal stem/progenitor cell may play a critical role in the pathological or regenerative response of the following insults: acid and bile resulting in reflux esophagitis; eosinophilic infiltration yielding eosinophilic esophagitis; exposure to bacterial and viral pathogens resulting in infectious esophagitis; and exposure to radiation resulting in radiation esophagitis. We used radiation targeted to the esophagus (as opposed to whole-body irradiation), as reflective of radiation therapy in humans, to determine whether *Krt15*-labeled cells might participate in or contribute to the regenerative response after radiation. We demonstrated that *Krt15*$^{+}$ cells are radioresistant. Furthermore, we demonstrate that esophagi from *Krt15*$^{-/-}$ mice regenerate more slowly than those from *Krt15*$^{+/+}$ mice following irradiation.

Under homeostatic conditions, ablation of *Krt15*$^{+}$ cells using a DTR system results in decreased basal cell proliferation leading to epithelial atrophy. Loss of *Krt15*-derived cells could be compensated potentially by other populations or even replenished by the generation of new *Krt15*$^{+}$ cells, thereby explaining possibly the modest phenotype observed in *Krt15-CrePR1 R26*^{iDTR} mice. Interactions between different populations, and even stem cell populations, have been reported in other tissues. For example, *Lgr5*$^{+}$ active stem cells are replenished by *Bmi1-CreER*$^{+}$ "reserve" stem cells in the small intestine following diphtheria toxin ablation of *Lgr5*$^{+}$ cells (38).

Heterogeneity in esophageal basal cells remains a controversial issue (10–12). Herein, we observed that *Krt15*$^{+}$ basal cells are not only functionally but also transcriptionally distinct from *Krt15*$^{-}$ basal cells. Enrichment for gene sets such as negative regulation of epithelial cell differentiation, stem cell proliferation, and cell fate specification as well as β-catenin binding in *Krt15*$^{+}$ basal cells support their potential roles in progenitor cell populations. The identification of a *Krt15*$^{+}$ long-lived progenitor cell population in the basal layer does not exclude the possibility of another stem/progenitor cell population. A hierarchical scheme was proposed with ITGA6^{hi}ITGB4^{hi}CD73^{+} stem cells, ITGA6^{hi}ITGB4^{hi}CD73^{-} early transit–amplifying cells, and ITGA6^{lo}ITGB4^{lo}CD73^{-} late transit–amplifying cells using a 3D organoid model (11). Interestingly, we observed that *Krt15*$^{+}$ basal cells express significantly higher *Itga6* and *Cd73* levels than *Krt15*$^{-}$ basal cells, suggesting that *Krt15*$^{+}$ basal cells identified herein could overlap with the previously described ITGA6^{hi}ITGB4^{hi}CD73^{+} cells. We previously identified a DNA label–retaining subpopulation of esophageal cells that displayed high CD34 expression (12). CD34^{+} cells express lower *Krt15* levels than CD34^{-} cells (data not shown), and *Krt15*$^{+}$ cells express lower levels of *Cd34*. We could then speculate that, like in other epithelia such as the skin and small intestine, more than 1 progenitor/stem cell population could be present in the mouse esophageal epithelium, although this requires further investigation.

Our data provide evidence for a long-lived subpopulation of esophageal epithelial basal cells that serve as progenitor cells. How does this reconcile with the premise that stem cells do not exist in the esophageal epithelium? Using a non–tissue-specific genetic driver, Doupe et al. concluded that the marked cells followed a stochastic/neutral competition model (10). The authors claimed the absence of slow-cycling or quiescent stem cells since they could not detect epithelial label–retaining cells. However, a recent publication suggests that, at least in the small intestine, label retention is not always a characteristic of quiescent or slow-cycling stem cells (39). Herein, we describe a long-lived population that could have been missed potentially by the use of a non–tissue-specific genetic approach. At the same time, our findings and those of Doupe et al. may not be necessarily mutually exclusive in that an uncommon long-lived progenitor cell population can give rise to all differentiated lineages as we demonstrate, but this population could coexist with neighboring basal cells that have the capacity to give rise to proliferating and differentiating cells with equal probability.

In summary, we have identified a novel long-lived *Krt15*$^{+}$ population with self-renewal and multipotency capacities. These cells are radioresistant and contribute to tissue regeneration following radiation-induced injury. These findings are, to our knowledge, the first genetic evidence of a bona fide long-lived progenitor cell population in the mouse esophageal epithelium and have significant implications in our understanding of the biology of widely prevalent esophageal diseases, such as acid/bile-induced esophagitis, eosinophilic esophagitis, and esophageal cancer (squamous cell carcinoma and adenocarcinoma).

Methods

Mouse models. *Krt15-CrePR1* (20) and *Krt15*$^{-/-}$ mice from VelociGene (KOMP Repository, Knockout mouse project; http://www.velocigene.com/komp/detail/10386) were provided by George Cotsarelis (University of Pennsylvania). *C57BL/6J* wild-type mice (WT), *Rosa26*$^{mTomato/mGFP}$ (*R26*$^{mT/mG}$) reporter mice (25), and inducible DTR *Rosa26*$^{LSL\text{-}DTR}$ (*R26*^{iDTR})

mice (32) were obtained from Jackson Laboratory. *Rosa26*^{Confetti} (*R26*^{Conf}) (26) mice were provided by Ben Stanger (University of Pennsylvania). *Krt15-CrePR1* mice were bred with *R26*$^{mT/mG}$, *R26*^{Conf}, or *R26*^{iDTR} mice to obtain *Krt15-CrePR1 R26*$^{mT/mG}$, *Krt15-CrePR1 R26*^{Conf}, and *Krt15-CrePR1 R26*^{iDTR} mice, respectively. All experiments were conducted with 6- to 10-week-old mice. Cre recombination was induced by i.p. injection of RU486 (Sigma-Aldrich). DTR activation was induced by i.p. injection of 1 μg diphtheria toxin (Sigma-Aldrich). The Institutional Animal Care and Use Committee of the University of Pennsylvania approved all animal studies. Detailed information regarding mouse experimental design and treatment is in Supplemental Methods.

Mouse irradiation experiments. *Krt15-CrePR1 R26*$^{mT/mG}$, WT (*Krt15*$^{+/+}$), and *Krt15*$^{-/-}$ mice were irradiated with a 12-Gy whole-body dose of radiation using a Gammacell 40 Cs^{137} Irradiation Unit. In *Krt15-CrePR1 R26*$^{mT/mG}$, Cre recombination was induced by i.p. RU486 injection prior to or following irradiation. WT and *Krt15*$^{-/-}$ mice were also irradiated with a 20-Gy esophageal-localized dose of irradiation. Briefly, CT scanning was performed on each animal to localize the trachea, which was used as an anatomical landmark to localize the esophagus. The esophagus was then irradiated using a 3-by-12-mm collimator in the neck region just above the rib cage with a 90° angle (20 Gy total administered at a speed of 1.65 Gy/min; Xstrahl Inc.). Acquisition of CT scan images and selection of the isocenter were performed using MuriSlice software (Supplemental Figure 6D). Esophageal-localized irradiation was performed using the Small Animal Radiation Research Platform (SARRP, University of Pennsylvania).

Fluorescence-activated cell sorting. Esophageal cells isolated from *Krt15-CrePR1 R26*$^{mT/mG}$ mice following Cre recombination were processed into single-cell suspensions (details in Supplemental Methods). Basal cells were labeled using PE/Cy5–CD29 antibody (1:50; 102219, BioLegend). DAPI was used to assess cell viability. The FACS sorter Influx (BD Biosciences) was used to sort the $CD29^{-}GFP^{-}$, $CD29^{-}GFP^{+}$, $CD29^{+}GFP^{-}$, and $CD29^{+}GFP^{+}$ cells. All experiments were performed at the University of Pennsylvania Flow Cytometry and Cell Sorting Facility. Cells were sorted in Advanced DMEM/F12 supplemented with penicillin-streptomycin, 1× Glutamax, 1× HEPES, 10 μM Y27632, and 0.2 U/ml DNase.

RNA-Seq. *Krt15-CrePR1 R26*$^{mT/mG}$ mice were injected with 1 mg of RU186 to induce Cre recombination (n = 3 mice). Twenty-four hours later, esophagi were harvested, and single-cell suspension from esophageal epithelial cells was prepared as described above. $CD29^{hi}GFP^{+}$ (*Krt15*$^{+}$) basal cells and $CD29^{hi}GFP^{-}$ (*Krt15*$^{-}$) basal cells were sorted. cDNA libraries were obtained from the sorted cells using SMART-Seq v4 Ultra Low Input RNA Kit for Sequencing (Clontech Laboratories) following the manufacturer's recommendations. Sequencing was performed using Illumina NextSeq500 (Molecular Biology Core Facilities, Dana-Farber Cancer Institute). Paired-end reads were aligned to the mouse genome mm9 using STAR 2.5. Alignments were performed using default parameters. Transcript expression quantification was performed using Cufflinks. Differential gene expression analysis was performed using the R package DESeq2. A final list of differentially expressed genes was obtained using an adjusted P value ≤ 0.05 and $\log_2$ fold change ≥ 2. Gene set enrichment analysis (GSEA) was performed on RNA-Seq data using Broad Institute guidelines as previously established (40). Significantly associated gene sets had nominal P values less than 0.05 and false discovery rates less than 0.25 with 1,000 permutations and weighted enrichment scoring. The RNA-Seq data were deposited in Gene Expression Omnibus (GEO GSE93331) and can be visualized at https://www.ncbi.nlm.nih.gov/geo/query/acc.cgi?token=gjefmeiyfjedhix&acc=GSE93331.

Details on esophageal epithelial cell isolation, immunohistochemistry and immunofluorescence, 3D organoid culture, human tissue samples, RNA extraction, quantitative PCR, Western blot, vibratome sectioning, and confocal imaging as well as statistical analyses are available in Supplemental Methods.

Author contributions

VG and AKR designed experiments with input from TCW, AJB, and HN. VG performed most of the experiments. AAL and AK helped with data acquisition. MMI and JRP helped with RNA-Seq analysis. VG, KEH, KAW, AL, QT, and CJL helped with data analysis. BR maintained the mouse colony. EPW performed the statistical analysis and mathematical modeling. AJKS provided formal histological and immunohistochemical analysis in a blinded fashion. The majority of manuscript writing was done by VG and AKR with contributions by other authors.

Acknowledgments

We are grateful to Ravikanth Maddipati, Samuel Asfaha, Daniel L. Worthley, and members of the Rustgi laboratory for discussions and comments on the manuscript. We thank the Molecular Pathology and Imaging Core, Human Microbial and Analytic Depository Core, Cell Culture and iPS Core, Genetic and Modified Mouse Core, and FACS/Sorting Core facility, University of Pennsylvania, as well as Molecular Biology Core Facilities, Dana-Farber Cancer Institute. This work was supported by NCI P01-CA098101 (to VG, AAL, MMI, KAW, BR, QT, HN, EPW, AJKS, AJB, and AKR), NIH/NIDDK P30-DK050306 Center of Molecular Studies in Digestive and Liver Diseases (to AKR), American Cancer Society (to AKR), Fonds de recherche en santé du Québec P-Giroux-27692 and P-Giroux-31601 (to VG), NIH/NCI F32-CA206264 (to AAL), NIH T32-DK007066-42 (to JRP), NIH/NIDDK K01-DK100485 (to KEH), NIH K01-DK103953 (to KAW), and NIH/NCI F30-CA175133 (to AL).

Address correspondence to: Anil K. Rustgi, 951 BRB II/III, Division of Gastroenterology, University of Pennsylvania, Perelman School of Medicine, 421 Curie Boulevard, Philadelphia, Pennsylvania 19104, USA. Phone: 215.898.0154; E-mail: anil2@mail.med.upenn.edu.

1. Zipori D. The nature of stem cells: state rather than entity. *Nat Rev Genet*. 2004;5(11):873–878.
2. Li L, Clevers H. Coexistence of quiescent and active adult stem cells in mammals. *Science*. 2010;327(5965):542–545.
3. Blanpain C, Fuchs E. Stem cell plasticity. Plasticity of epithelial stem cells in tissue regeneration. *Science*. 2014;344(6189):1242281.
4. Rezza A, Sennett R, Rendl M. Adult stem cell niches: cellular and molecular components. *Curr Top Dev Biol*. 2014;107:333–372.
5. Sato T, et al. Paneth cells constitute the niche for Lgr5 stem cells in intestinal crypts. *Nature*. 2011;469(7330):415–418.
6. Aoki R, et al. Foxl1-expressing mesenchymal cells constitute the intestinal stem cell niche. *Cell Mol Gastroenterol Hepatol*. 2016;2(2):175–188.
7. Hsu YC, Fuchs E. A family business: stem cell

progeny join the niche to regulate homeostasis. *Nat Rev Mol Cell Biol*. 2012;13(2):103–114.
8. Acar M, et al. Deep imaging of bone marrow shows non-dividing stem cells are mainly perisinusoidal. *Nature*. 2015;526(7571):126–130.
9. Croagh D, Phillips WA, Redvers R, Thomas RJ, Kaur P. Identification of candidate murine esophageal stem cells using a combination of cell kinetic studies and cell surface markers. *Stem Cells*. 2007;25(2):313–318.
10. Doupé DP, et al. A single progenitor population switches behavior to maintain and repair esophageal epithelium. *Science*. 2012;337(6098):1091–1093.
11. DeWard AD, Cramer J, Lagasse E. Cellular heterogeneity in the mouse esophagus implicates the presence of a nonquiescent epithelial stem cell population. *Cell Rep*. 2014;9(2):701–711.
12. Kalabis J, et al. A subpopulation of mouse esophageal basal cells has properties of stem cells with the capacity for self-renewal and lineage specification. *J Clin Invest*. 2008;118(12):3860–3869.
13. Marques-Pereira JP, Leblond CP. Mitosis and differentiation in the stratified squamous epithelium of the rat esophagus. *Am J Anat*. 1965;117:73–87.
14. Seery JP. Stem cells of the oesophageal epithelium. *J Cell Sci*. 2002;115(pt 9):1783–1789.
15. Scharenberg CW, Harkey MA, Torok-Storb B. The ABCG2 transporter is an efficient Hoechst 33342 efflux pump and is preferentially expressed by immature human hematopoietic progenitors. *Blood*. 2002;99(2):507–512.
16. Rompolas P, et al. Spatiotemporal coordination of stem cell commitment during epidermal homeostasis. *Science*. 2016;352(6292):1471–1474.
17. Van Keymeulen A, Blanpain C. Tracing epithelial stem cells during development, homeostasis, and repair. *J Cell Biol*. 2012;197(5):575–584.
18. Rustgi AK, El-Serag HB. Esophageal carcinoma. *N Engl J Med*. 2014;371(26):2499–2509.
19. Furuta GT, Katzka DA. Eosinophilic esophagitis. *N Engl J Med*. 2015;373(17):1640–1648.
20. Morris RJ, et al. Capturing and profiling adult hair follicle stem cells. *Nat Biotechnol*. 2004;22(4):411–417.
21. Ito M, et al. Stem cells in the hair follicle bulge contribute to wound repair but not to homeostasis of the epidermis. *Nat Med*. 2005;11(12):1351–1354.
22. Li S, et al. A keratin 15 containing stem cell population from the hair follicle contributes to squamous papilloma development in the mouse. *Mol Carcinog*. 2013;52(10):751–759.
23. Wang GY, Wang J, Mancianti ML, Epstein EH. Basal cell carcinomas arise from hair follicle stem cells in Ptch1(+/–) mice. *Cancer Cell*. 2011;19(1):114–124.
24. Tai G, et al. Cytokeratin 15 marks basal epithelia in developing ureters and is upregulated in a subset of urothelial cell carcinomas. *PLoS ONE*. 2013;8(11):e81167.
25. Muzumdar MD, Tasic B, Miyamichi K, Li L, Luo L. A global double-fluorescent Cre reporter mouse. *Genesis*. 2007;45(9):593–605.
26. Snippert HJ, et al. Intestinal crypt homeostasis results from neutral competition between symmetrically dividing Lgr5 stem cells. *Cell*. 2010;143(1):134–144.
27. Liu Y, Lyle S, Yang Z, Cotsarelis G. Keratin 15 promoter targets putative epithelial stem cells in the hair follicle bulge. *J Invest Dermatol*. 2003;121(5):963–968.
28. Leung Y, Kandyba E, Chen YB, Ruffins S, Kobielak K. Label retaining cells (LRCs) with myoepithelial characteristic from the proximal acinar region define stem cells in the sweat gland. *PLoS ONE*. 2013;8(9):e74174.
29. Messier B, Leblond CP. Cell proliferation and migration as revealed by radioautography after injection of thymidine-H3 into male rats and mice. *Am J Anat*. 1960;106:247–285.
30. van der Flier LG, et al. Transcription factor achaete scute-like 2 controls intestinal stem cell fate. *Cell*. 2009;136(5):903–912.
31. Croagh D, Thomas RJ, Phillips WA, Kaur P. Esophageal stem cells — a review of their identification and characterization. *Stem Cell Rev*. 2008;4(4):261–268.
32. Saito M, et al. Diphtheria toxin receptor-mediated conditional and targeted cell ablation in transgenic mice. *Nat Biotechnol*. 2001;19(8):746–750.
33. Yan KS, et al. The intestinal stem cell markers Bmi1 and Lgr5 identify two functionally distinct populations. *Proc Natl Acad Sci U S A*. 2012;109(2):466–471.
34. Tao S, et al. Wnt activity and basal niche position sensitize intestinal stem and progenitor cells to DNA damage. *EMBO J*. 2015;34(5):624–640.
35. Asfaha S, et al. Krt19(+)/Lgr5(–) cells are radioresistant cancer-initiating stem cells in the colon and intestine. *Cell Stem Cell*. 2015;16(6):627–638.
36. Wilson TM, et al. Differential cellular expression of the human MSH2 repair enzyme in small and large intestine. *Cancer Res*. 1995;55(22):5146–5150.
37. Tomé S, et al. Tissue-specific mismatch repair protein expression: MSH3 is higher than MSH6 in multiple mouse tissues. *DNA Repair (Amst)*. 2013;12(1):46–52.
38. Tian H, et al. A reserve stem cell population in small intestine renders Lgr5-positive cells dispensable. *Nature*. 2011;478(7368):255–259.
39. Li N, Nakauka-Ddamba A, Tobias J, Jensen ST, Lengner CJ. Mouse label-retaining cells are molecularly and functionally distinct from reserve intestinal stem cells. *Gastroenterology*. 2016;151(2):298–310.e7.
40. Subramanian A, et al. Gene set enrichment analysis: a knowledge-based approach for interpreting genome-wide expression profiles. *Proc Natl Acad Sci U S A*. 2005;102(43):15545–15550.